

# Towards Fully Passive Plug and Play Time-Bin Quantum Key Distribution over Multi-Mode Channels

Ramy Tannous<sup>1</sup>, Wilson Wu<sup>1</sup>, Stéphane Vinet<sup>1</sup>, Chithrabhanu Perumangatt<sup>2</sup>, Dogan Sinar<sup>1</sup>, Alexander Ling<sup>2,3</sup>, Thomas Jennewein<sup>1</sup>

<sup>1</sup> Institute for Quantum Computing and Department of Physics & Astronomy, University of Waterloo, 200 University Ave W, Waterloo, Ontario, N2L 3G1, Canada

<sup>2</sup> Centre for Quantum Technologies, 3 Science Drive 2, National University of Singapore 117543 Singapore

<sup>3</sup> Department of Physics, Faculty of Science, National University of Singapore, 2 Science Drive 3, 117551 Singapore

**Abstract.** Phase stabilization of distant quantum time-bin interferometers can be a major challenge for quantum communication networks, and is typically achieved by exchanging reference optical signals, which can be particularly challenging for free-space communication channels. We demonstrate a novel solution that utilizes reference frame independent time-bin quantum key distribution that completely avoids the need for active relative phase stabilization of the remote interferometers. We realized a proof of concept experiment using a source of hybrid entanglement with polarization and time-bin, and show a sustained asymptotic secure key rate of greater than 0.06 bits/coincidence over a 15 m multi-mode fiber optical channel. This is achieved without the use of mode filtering, adaptive optics, active basis selection, nor active phase alignment. This system can therefore be considered a passive plug and play self-compensating solution that is suitable for spatially multi-mode channels, and improves the viability of time-bin quantum communication links over challenging channels such as airborne, ground to space, and multi-mode fibers.

Time-bin encoding for quantum key distribution (QKD) continues to be the encoding of choice for optical-fiber quantum networks [1, 2, 3]. More recently, there have been demonstrations of time-bin over free space channels [4], enabled by the development of multi-mode field widened interferometers [5]. Despite recent efforts in improving the short and long-term phase stability of these interferometers [6], it remains experimentally challenging. Active systems are typically required to align the sender and receiver interferometers' relative phase which creates additional technical overhead to successfully perform time-bin QKD [7, 8, 9]. In addition, using active phase alignment over a fluctuating channel, such as a turbulent atmosphere, is difficult since a reference laser would suffer from random intensity fluctuations. Conversely, plug & play QKD systems provide a passive self-compensating solution and are typically based on retroreflection [10, 11]. However, we make use of a reference frame independent

quantum key distribution (RFI-QKD) protocol that avoids the requirement for active phase locking of the two interferometers, and is applicable to both prepare-and-measure and entanglement schemes [12]. The specific benefit of RFI-QKD protocols is that while the relative phase between the two interferometers is allowed to drift, the channel purity between the two key exchange parties can still be determined, provided the phase drift is relatively “slow” to allow for the sufficient estimation of the channel parameters. Recently, several time-bin RFI-QKD demonstrations were performed over free space and optical fiber channels [13, 14, 15]. However, the use of single-mode interferometers and active basis choice have their disadvantages. The use of single-mode interferometers over a free space channel can result in significant photon throughput losses, and thus affect the overall system performance, unless an adaptive optics system is used which increases the system overhead. In addition, active basis and phase encoding requires effort in pulse synchronization that can present experimental challenges for moving platforms such as planes [16], drones, or satellites [17, 18], where resources may be limited.

In this work, we demonstrate a fully passive time-bin quantum communication scheme that has no active basis selection, mode filtering, adaptive optics, nor interferometer stabilization. To achieve this, we utilize the entanglement as the source of randomness reducing the required operational overhead of the implementation, and use interferometers shown to easily perform time-bin QKD over a free space channel [4]. While the use of the 6-state 4-state time-bin RFI-QKD removes the need for active interferometer phase stabilization. Due to the simplicity of our scheme, it can be easily adapted for free space quantum channels particularly moving platforms. Despite the use of a spatially multi-mode channel, our system is able to achieve quantum bit error rates (QBER) below 5% and 7% for the key distillation basis and phase estimation basis, respectively, while maintaining a continuous asymptotic key rate of greater than 0.06 bits/coincidence.

We utilize the 6-state 4-state time-bin RFI-QKD protocol that is based on an entangled photon source (EPS) [19] where one photon is converted from polarization to time-bin [20]. The state shared between Alice and Bob is thus

$$|\psi_{AB}\rangle = \frac{1}{\sqrt{2}} (|H\mathcal{E}\rangle + e^{i\phi_{AB}} |V\mathcal{L}\rangle), \quad (1)$$

where  $\phi_{AB}$  is the relative phase between Alice and Bob;  $H$ ,  $V$  are the horizontal and vertical polarizations respectively; and  $\mathcal{E}$ ,  $\mathcal{L}$  are the early and late time-bins respectively. The particular benefit of this hybrid entangled state is the relative ease of producing a 6-state analyzer for the polarization encoded photons, while a 4-state analyzer for time-bin photons is an unbalanced interferometer. Alice performs a 6-state polarization measurement on the first qubit, measuring in the  $Z_A$ ,  $X_A$ , and  $Y_A$  bases, while Bob makes a 4-state time-bin measurement on the other qubit measuring in the  $Z_B$  and  $X_B$  bases. In our implementation, the computational basis is the horizontal-vertical polarization basis ( $Z_A$ ) for Alice and the early-late ( $Z_B$ ) basis for Bob, and are the fixed bases for the RFI protocol that are used to generate the keymap.‡

‡ Although we use an entanglement based approach, this scheme could easily be adapted for a prepare-

As shown in [19], a key can be generated despite the phase drifts provided that strong correlations are maintained in between the polarization superposition bases and the time-bin superposition basis, which are found in the  $C$ -parameter given by

$$C = \sqrt{\langle X_A \otimes X_B \rangle^2 + \langle Y_A \otimes X_B \rangle^2}, \quad (2)$$

where  $0 \leq C \leq 1$  allows the users to estimate the channel quality with  $C = 1$  indicating a maximally entangled state or perfect channel [19]. Monitoring the superposition coincidences between the polarization superposition bases and the time-bin superposition basis ( $C$ -parameter) allows the users to estimate the channel quality.

During key exchange,  $\phi_{AB}$  can take any value and can drift during key generation and exchange, provided it does not change too rapidly [21, 22]. The degree to which the phase can change is a function of the photon detection rate and timing resolution of the system. To quantify the effects of a rapidly changing  $\phi_{AB}$  we use a Monte Carlo simulation. We consider  $N$  signals sent by the EPS to Alice and Bob that arrive evenly spaced over a time period  $t_N$ . The instantaneous phase of the entangled state is  $\phi(\tau n)$ , where  $n \in [0, N]$ , while the total phase variation over the measurement time interval is given by  $\phi(t_N)$ . Numerically using the Qutip package [23, 24], we produce  $N$  entangled states (1) each with a phase  $\phi(\tau n)$ . Then for each  $n$  entangled state, we calculate the detection probabilities of the POVM's (e.g.  $XX_{++}$ ,  $XX_{+-}$ ,  $XX_{-+}$ ,  $XX_{--}$ ) for each basis that is involved in calculating the  $C$ -parameter. Since  $\phi(t)$  is changing, these probabilities should vary with time (and phase). With the probabilities calculated from every  $n$  entangled state, a pseudorandom number generator determines the detection results of a single photon event. This is done independently for each event. The result is then counted and statistics are accumulated for the total  $N$  entangled pairs. Once complete, an experimental expectation value approximation is calculated using equation (2) of [19] for each basis from which a value for the average  $C$ -parameter over the time interval is determined. This process is repeated  $i$  times for each  $\phi(t_N)$  and the average value of the distribution is taken to be the value of  $C(t_N)$  with error bounds being the standard deviation of the each distribution.

Figure 1 shows a sketch of the experimental setup used for the time-bin RFI-QKD proof of principle demonstration, where we perform the adapted 6-state 4-state protocol [19]. Our experiment consists of an entangled photon source [25], a local 6-state polarization measurement, a polarization to time-bin converting interferometer, a quantum channel, a time-bin analyzing interferometer, and detection of single photons, including time-tagging. Coincidence and correlation data is done on a computer during post-processing. The EPS creates polarization entangled photon pairs in the state  $|\psi_{AB}\rangle = \frac{1}{\sqrt{2}} (|H_A H_B\rangle + e^{i\phi_{AB^*}} |V_A V_B\rangle)$ , where  $\phi_{AB^*}$  is a random phase introduced by the EPS. From each entangled pair, the idler photon is measured using a 6-state polarization measurement [19], while the signal photon is converted to time-bin encoding before being sent across a 15 m multi-mode fiber. The polarization to time-bin converter (PTC) is an and-measure type scheme where the sender produces 6 states while the receiver measures 4 states or vice-versa.

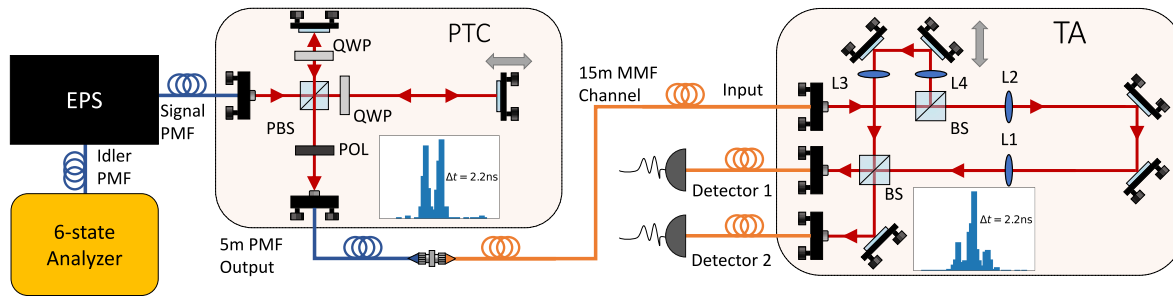


Figure 1: Experimental setup of the time-bin RFI-QKD proof of principle demonstration. An entangled photon source (EPS) creates polarization entangled photon pairs at 785 nm (signal) and 842 nm (idler) via spontaneous parametric downconversion. The idler photon is measured at a local 6-state polarization analyzer, while the signal photon is converted to time-bin encoding by the polarization to time-bin converter (PTC) and sent across a 15 m multi-mode fiber (MMF) optic channel to a receiver, the time-bin analyzer (TA), that performs a 4-state time-bin measurement. A time tagging unit is used to record detection events (not shown). Both the PTC and TA interferometers have a path separation of 2.2 ns. The TA is a  $4f$  field widened interferometer with multi-mode fiber inputs and outputs. No active phase compensation is used to maintain a phase reference between the two interferometers. A piezoelectric actuator is inserted in the TA short path to induce a phase drift. HWP: half-waveplate, QWP: quarter-waveplate, L: lens, POL: polarizer, PMF: polarization maintaining fiber, PBS: polarizing beam splitter, BS: 50:50 beam splitter.

unbalanced Michelson interferometer shown in figure 1. A polarizing beam splitter in combination with quarter-waveplates are used to maximize the signal sent to the output port of the Michelson interferometer. The PTC is designed such that the horizontal polarized light takes the short path ( $H \rightarrow \mathcal{E}$ ) and vertically polarized light takes the long path, ( $V \rightarrow \mathcal{L}$ ) which creates the entangled state in (1). Thus any photon in a polarization superposition would create a superposition of both interferometer paths in the PTC. The polarization information of the photons is removed at the output of the PTC by placing a polarizer at  $45^\circ$  with respect to the horizontal and vertical polarizations. The separation of the time-bins is given by the path difference of the PTC which is approximately 2.2 ns.

By passing through the PTC, the polarized signal photons are converted to appropriate time-bin states and are then sent across the 15 m multi-mode fiber (Corning InfiniCor 300 62.5/125). The channel is a graded-index fiber which has a core size of  $62.5 \mu\text{m}$  and a numerical aperture of 0.275. The estimated maximum modal dispersion for this fiber is  $0.353 \text{ ns km}^{-1}$  which amounts to a negligible 5.2 ps over the 15 m length. A field widened multi-mode time-bin analyzer (TA) is used to measure the time-bin encoded photons after they pass through the quantum channel [4]. The optical layout of the TA is shown in figure 1. The TA uses a  $4f$  imaging system in each arm. No phase stabilization is used to obtain a phase reference between the PTC and the TA. In fact,

the relative phase of the PTC and TA are allowed to drift with ambient noise. In some photon exchanges, a piezoelectric actuator is used to deliberately induce a phase change in the TA to demonstrate the robustness of the protocol (figure 3). The outputs of the TA are coupled into multi-mode fibers connected to single photon avalanche diodes. A time tagging unit is used to record the detection events and coincidence analysis is done to calculate the correlations in the various bases. The use of a single time tagging unit is not secure and two independent time tagging units, one each at Alice and Bob, are needed to properly perform QKD. However, the single time tagging unit is sufficient for this demonstration.

The overall number of coincidences measured in our proof of concept experiment is about 9000 coincidence/s. The EPS has an intrinsic pair production rate of approximately  $10 \times 10^6$  pairs/s. However, the heralding efficiency of the source  $\approx 20\%$ , which includes the losses due to fiber coupling into the PMF, reduces the measured pair rate. Furthermore, the losses contributed by the PTC and TA, and the detector efficiencies also reduce the overall number of coincidences measured. The PTC throughput is measured to be 35.4% including fiber coupling into the output PMF, however it is intrinsically reduced by 50% due to the polarizer that eliminates the polarization signature of each time-bin. The 15 m multi-mode channel has a throughput of 86.1%, while the TA has throughput of 67.0%, including coupling into the multi-mode fibers, but not including the detector efficiency. The 6-state polarization analyzer at Alice has an approximate throughput of 49.6% across all six paths, again not including the detector efficiencies. The throughput of the PTC, TA, quantum channel, and 6-state analyzer were measured using a laser and power meter. Experimentally, the total combined efficiencies, including single photon detector efficiency, are 9.3% for the idler photons measured by Alice and 1.1% for the signal photons measured by Bob.

The results of our demonstration are shown in figure 2 and figure 3. Here we describe two experimental scenarios; (i) the system and interferometers are allowed to drift due to fluctuations from the environment, (ii) a piezoelectric actuator in the TA is driven to produce a constant phase change of  $0.1 \text{ rad s}^{-1}$ . Despite the lack of active compensation of the two interferometers' relative phase, average visibilities of  $88.5 \pm 1.5\%$  and  $86.5 \pm 1.7\%$  are observed in the phase-dependent superposition basis for scenarios (i) and (ii) respectively. This corresponds to an average QBER in the superposition basis of  $5.8 \pm 0.8\%$  and  $6.8 \pm 0.9\%$  for scenarios (i) and (ii) respectively, while the QBER in the computational basis is  $4.2 \pm 0.9\%$  and  $3.4\% \pm 0.6\%$  for scenarios (i) and (ii) respectively. The visibility of the superposition basis is derived from the  $C$ -parameter and is a combination of the visibility of the EPS (95%), the PTC interferometer (99%), and the TA interferometer (93%). Combined, the estimated visibility for the superposition basis is 87% and gives a combined expected QBER of approximately 6.5%, which agrees with the experimentally observed values. Other errors, such as waveplate errors and imperfections in the beam splitters are not accounted for but can contribute to the error in our demonstration.

With this  $C$ -parameter, an asymptotic key rate was calculated following the

analysis of [19]. The number of secret key bits per coincidence detection at the asymptotic limit is estimated to be 0.063 bits/coincidence and 0.063 bits/coincidence ((i) and (ii) respectively) compared to the maximum achievable rate for our system of 0.167 bits/coincidence. Despite the varying phase, there is no significant variation in QBER and asymptotic key rate in figures 2b, 3b.

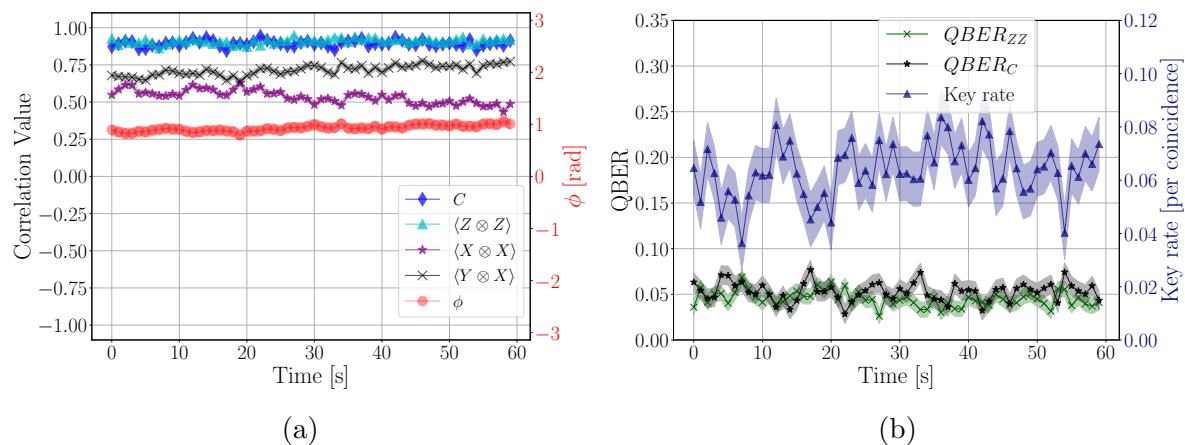


Figure 2: **(a)** Measured correlation values and phase as a function of time for a 60 s link (scenario (i)).  $\phi$  is the relative phase difference between the two interferometers. **(b)** The corresponding asymptotic key rate and QBER. All errors are shown as shaded regions and are approximated by Poissonian count errors.

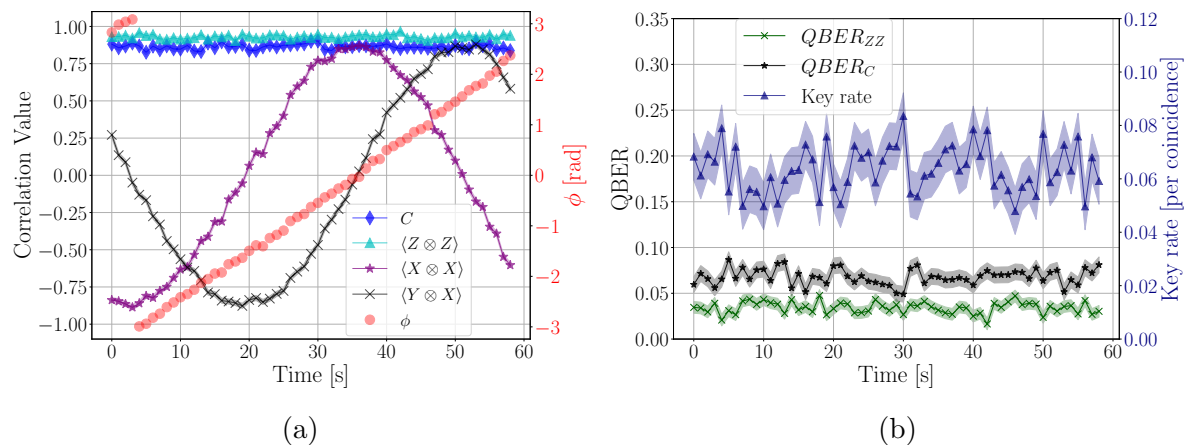


Figure 3: **(a)** Measured correlation values and phase as a function of time for a 60 s demonstration while a piezo actuator is inducing a phase change ( $0.1 \text{ rad s}^{-1}$ ) in the TA (scenario (ii)). **(b)** The corresponding asymptotic key rate and QBER. All errors are shown as shaded regions and are approximated by Poissonian count errors.

Clearly, in figures 2a, 3a the  $C$ -parameter is shown to be phase independent and constant throughout the entire photon exchange. This is achieved despite deliberate phase variation between the PTC and TA (figure 3a). We use our Monte Carlo

simulation to estimate the effects of a phase change for our system that measures about 3000 coincidences ( $N = 3000$ ) in the superposition basis during a 1 s ( $t_N = 1$ ) measurement time interval (figure 4). The tolerated relative phase drift is approximately  $0.512 \text{ rad s}^{-1}$  before a 5% reduction in the asymptotic key rate. This tolerance can be increased by having more coincidences per measurement time interval or by reducing the measurement time, i.e. a faster measurement system. A longer measurement time will increase the number of photon detections, but increase the smearing effect and cause a larger drop in key rate for the same phase change rate. In figure 4 we compare our Monte Carlo simulation to a modified version equation (17) from [26]. The modifications are necessary to match the definition of  $C$  used in the 6-state 4-state protocol [19].

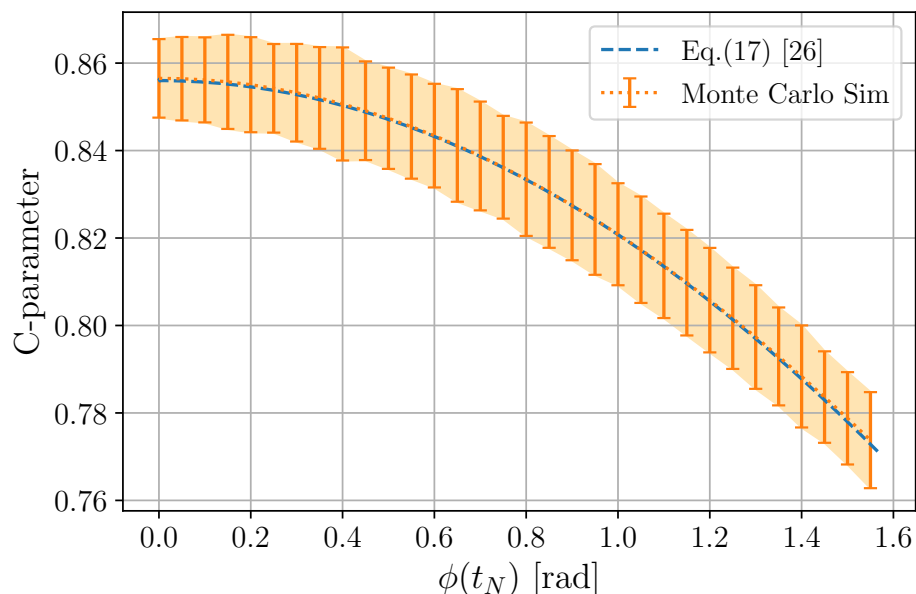


Figure 4: Change in the value of the  $C$ -parameter as a function of phase variation over a fixed time period ( $\phi(t_N)$ ). The error bars are the standard deviation of the Monte Carlo distribution and demonstrate the statistical nature of the  $C$ -parameter that is not captured by equation (17) of [26]. The error bars can be reduced by increasing the number of photons collected in the time  $t_N$ . Here  $i = 300$  for each  $\phi(t_N)$ .

Furthermore, we perform an indicative finite key rate estimation using the approach from [26] that analyzed a 6-state entanglement-based RFI protocol. For our analysis, we make the assumption that the correlations of the entangled state shared between Alice and Bob are symmetric ( $\langle X_A \otimes X_B \rangle^2 = \langle Y_A \otimes Y_B \rangle^2$  and  $\langle Y_A \otimes X_B \rangle^2 = \langle X_A \otimes Y_B \rangle^2$ ) such that we can take the 6-state 4-state  $C$ -parameter ( $C_{64}$ ) and relate it to the 6-state  $C_{66}$  as  $C_{66} = 2C_{64}^2$ . Proper investigation of this assumption is a topic of further study. In addition, future work will be done to use modern numerical finite size key analysis [27]. Using equations (2) and (3) from [26], the expression for the secret-key length

secure against coherent attack for our system given by

$$r_N = \frac{n}{N} \left[ 1 - I_E(Q', C') - n_Q f h(Q') - \log_2 \frac{2}{\varepsilon_{\text{EC}}} - 2 \log_2 \frac{1}{\varepsilon_{\text{PA}}} - 7 \sqrt{\frac{\log_2(2/\bar{\varepsilon})}{n}} - \frac{30}{N} \log_2(N+1) \right], \quad (3)$$

where  $N$  is the total raw key (signals sent by Alice and detected by Bob),  $n$  is the number of detections in the key map (computational) basis,  $C'$  ( $Q'$ ) is the observed  $C$ -parameter (error rate in the key map basis) modified to account for finite statistics [26], and  $I_E$  is the upper bound on the information that Eve can gain. The other finite size parameters are found in table 1. For scenario (i), we considered the entire 60s in determining the  $C$ -parameter and QBER. This gave a total number of coincidences of 487936, a computational basis QBER of 4.2% and a  $C_{64}$ -parameter of 0.8845. With these parameters and assuming perfect error correction, we calculate a secret key fraction of 0.00571, which amounts to 2785 secret bits from the total raw key. For (ii), considering the entire 60s link would not produce any key as the smearing of the  $C$ -parameter would be too great. However, shorter integration times would not produce positive key due to low photon statistics. For an error correction factor of  $f = 1.2$ , no positive secret key is achievable. However for an error correction factor of  $f = 1.0$ , the only positive key achieved for (ii) while using all other parameter values of table 1, is from one 13s block that has a secret key fraction of 0.00217 or 229 secret bits from the 120649 coincidences of the 13s block. It is apparent that the coincidence count rates need to be improved in order to produce a secret key that is similar with state of the art systems reported by the literature [14, 15].

Table 1: Parameters of the finite size secret key analysis.

Parameter	Description	Value
$\bar{\varepsilon}$	Smooth min entropy estimation error	$2.5 \times 10^{-9}$
$\varepsilon_{\text{EC}}$	Error correction failure probability	$2.5 \times 10^{-9}$
$\varepsilon_{\text{PA}}$	Privacy amplification failure probability	$2.5 \times 10^{-9}$
$\varepsilon_{\text{PE}}$	Parameter estimation failure probability	$2.5 \times 10^{-9}$
$n_Q$	Fraction of computational basis used to estimate the QBER	0.1
$f$	Error correction factor	1.2

To our knowledge, our results are of the first fully passive time-bin RFI-QKD implementation over a multi-mode fiber. We demonstrated time-bin QKD without the need for any active phase stabilization of the sender and receiver interferometers, and without actively correcting for spatial mode distortions. Overall this system could therefore be considered a plug and play QKD system. While using a hybrid entanglement-based 6-state 4-state RFI-QKD protocol, we observed error rates of less than 7% in the superposition basis, a continuous asymptotic key rate of above 0.06 bits/coincidence, and when accounting for finite size, achieved an estimated key

length of 2785 secret bits over 60s. Our results are of great practical importance since the ability to distribute entanglement correlations with time-bin encoded photons can ease the deployment of quantum networks, entanglement distribution experiments, and quantum sensing applications [28]. Furthermore, the purely passive scheme is particularly suitable for QKD with moving platforms where the use of multi-mode interferometers are desirable compared to single-mode interferometers due to better pointing requirements and optical throughput. The next steps are to improve the performance of the system in terms of photon throughput by working with a source that is optimized for the apparatus wavelength and bandwidth, and increasing the EPS heralding efficiency and visibility to near unity [29]. In addition, improving the performance of the field widened interferometers with a better optical design and custom optics to reduce the overall QBER of the system, for instance using a compact optical layout [6]. Further theoretical studies on the robustness of the protocol are to be conducted, particularly against rapid phase fluctuations and finite size effects.

## Acknowledgments

The authors would like to thank Dr. Norbert Lütkenhaus and Scott Johnston for discussions on the analysis. The authors are grateful for the support from the Canada Foundation for Innovation, the Ontario Research Fund, the Canadian Institute for Advanced Research, the Natural Sciences and Engineering Research Council of Canada, Industry Canada, and the Research Centres of Excellence program supported by the National Research Foundation (NRF) Singapore and the Ministry of Education, Singapore. RT would like to thank the NSERC CGS-D for personal funding.

## References

- [1] J. Brendel, N. Gisin, W. Tittel, and H. Zbinden. Pulsed Energy-Time Entangled Twin-Photon Source for Quantum Communication. *Physical Review Letters*, 82(12):2594–2597, March 1999.
- [2] W. Tittel, J. Brendel, H. Zbinden, and N. Gisin. Quantum Cryptography Using Entangled Photons in Energy-Time Bell States. *Physical Review Letters*, 84(20):4737–4740, May 2000.
- [3] R. T. Thew, S. Tanzilli, W. Tittel, H. Zbinden, and N. Gisin. Experimental investigation of the robustness of partially entangled qubits over 11 km. *Physical Review A*, 66(6):062304, December 2002.
- [4] Jeongwan Jin, Jean-Philippe Bourgoin, Ramy Tannous, Sascha Agne, Christopher J Pugh, Katanya B Kuntz, Brendon L Higgins, and Thomas Jennewein. Genuine time-bin-encoded quantum key distribution over a turbulent depolarizing free-space channel. *Optics express*, 27(26):37214–37223, 2019.
- [5] Jeongwan Jin, Sascha Agne, Jean-Philippe Bourgoin, Yanbao Zhang, Norbert Lütkenhaus, and Thomas Jennewein. Demonstration of analyzers for multimode photonic time-bin qubits. *Phys. Rev. A*, 97(4):043847, April 2018. Publisher: American Physical Society.
- [6] Clinton Cahall, Nurul T. Islam, Daniel J. Gauthier, and Jungsang Kim. Multi-mode Time-delay Interferometer for Free-space Quantum Communication. *Physical Review Applied*, 13(2):024047, February 2020. arXiv: 1908.00852.
- [7] C Gobby, aZL Yuan, and AJ Shields. Quantum key distribution over 122 km of standard telecom fiber. *Applied Physics Letters*, 84(19):3762–3764, 2004.

- [8] ZL Yuan and AJ Shields. Continuous operation of a one-way quantum key distribution system over installed telecom fibre. *Optics express*, 13(2):660–665, 2005.
- [9] Erik Fitzke, Lucas Bialowons, Till Dolejsky, Maximilian Tippmann, Oleg Nikiforov, Thomas Walther, Felix Wissel, and Matthias Gunkel. Scalable network for simultaneous pairwise quantum key distribution via entanglement-based time-bin coding. *PRX Quantum*, 3(2):020341, 2022.
- [10] William S Rabinovich, Rita Mahon, Mike S Ferraro, Peter G Goetz, Mark Bashkansky, Rachel E Freeman, John Reintjes, and James L Murphy. Free space quantum key distribution using modulating retro-reflectors. *Optics Express*, 26(9):11331–11351, 2018.
- [11] Xingyu Wang, Wei Liu, Tianyi Wu, Chang Guo, Yijun Zhang, Shanghong Zhao, and Chen Dong. Free space measurement device independent quantum key distribution with modulating retro-reflectors under correlated turbulent channel. *Entropy*, 23(10):1299, 2021.
- [12] Anthony Laing, Valerio Scarani, John G Rarity, and Jeremy L O’Brien. Reference-frame-independent quantum key distribution. *Physical Review A*, 82(1):012304, 2010.
- [13] Huan Chen, Jipeng Wang, Bangying Tang, Zhenhua Li, Bo Liu, and Shihai Sun. Field demonstration of time-bin reference-frame-independent quantum key distribution via an intracity free-space link. *Opt. Lett.*, 45(11):3022, June 2020.
- [14] Bao Feng, Ziyang Zhao, Shunyu Yang, Tianqi Dou, Zhenhua Li, Jipeng Wang, Zhongqi Sun, Fen Zhou, Yanxin Han, Yuqing Huang, and Haiqiang Ma. Four-state reference-frame-independent quantum key distribution using heralded pair-coherent sources with source flaws. *Optoelectronics Letters*, 17(10):636–640, October 2021.
- [15] Bang-Ying Tang, Huan Chen, Ji-Peng Wang, Hui-Cun Yu, Lei Shi, Shi-Hai Sun, Wei Peng, Bo Liu, and Wan-Rong Yu. Free-running long-distance reference-frame-independent quantum key distribution. *npj Quantum Information*, 8(1):1–8, September 2022. Number: 1 Publisher: Nature Publishing Group.
- [16] Christopher J. Pugh, Sarah Kaiser, Jean-Philippe Bourgoin, Jeongwan Jin, Nigar Sultana, Sascha Agne, Elena Anisimova, Vadim Makarov, Eric Choi, Brendon L. Higgins, and Thomas Jennewein. Airborne demonstration of a quantum key distribution receiver payload. *Quantum Sci. Technol.*, 2(2):024009, June 2017. arXiv:1612.06396 [quant-ph].
- [17] Sheng-Kai Liao, Wen-Qi Cai, Wei-Yue Liu, Liang Zhang, Yang Li, Ji-Gang Ren, Juan Yin, Qi Shen, Yuan Cao, Zheng-Ping Li, Feng-Zhi Li, Xia-Wei Chen, Li-Hua Sun, Jian-Jun Jia, Jin-Cai Wu, Xiao-Jun Jiang, Jian-Feng Wang, Yong-Mei Huang, Qiang Wang, Yi-Lin Zhou, Lei Deng, Tao Xi, Lu Ma, Tai Hu, Qiang Zhang, Yu-Ao Chen, Nai-Le Liu, Xiang-Bin Wang, Zhen-Cai Zhu, Chao-Yang Lu, Rong Shu, Cheng-Zhi Peng, Jian-Yu Wang, and Jian-Wei Pan. Satellite-to-ground quantum key distribution. *Nature*, 549(7670):43–47, September 2017.
- [18] Hugh Podmore, I. D’Souza, J. Cain, T. Jennewein, B. L. Higgins, Y. S. Lee, A. Koujelev, D. Hudson, and A. McColgan. QKD terminal for Canada’s Quantum Encryption and Science Satellite (QEYSSat). In Zoran Sodnik, Bruno Cugny, and Nikos Karafolas, editors, *International Conference on Space Optics — ICSO 2020*, page 17, Online Only, France, June 2021. SPIE.
- [19] Ramy Tannous, Zhangdong Ye, Jeongwan Jin, Katanya B Kuntz, Norbert Lütkenhaus, and Thomas Jennewein. Demonstration of a 6 state-4 state reference frame independent channel for quantum key distribution. *Applied Physics Letters*, 115(21):211103, 2019.
- [20] Xiao-song Ma, Angie Qarry, Johannes Kofler, Thomas Jennewein, and Anton Zeilinger. Experimental violation of a bell inequality with two different degrees of freedom of entangled particle pairs. *Physical Review A*, 79(4):042101, 2009.
- [21] Fumin Wang, Pei Zhang, Xiaoli Wang, and Fuli Li. Valid conditions of the reference-frame-independent quantum key distribution. *Physical Review A*, 94(6):062330, 2016.
- [22] Juhwan Yoon, Tanumoy Pramanik, Byung-Kwon Park, Young-Wook Cho, Sang-Yun Lee, Sangin Kim, Sang-Wook Han, Sung Moon, and Yong-Su Kim. Experimental comparison of various quantum key distribution protocols under reference frame rotation and fluctuation. *Optics Communications*, 441:64–68, June 2019.

- [23] J Robert Johansson, Paul D Nation, and Franco Nori. Qutip: An open-source python framework for the dynamics of open quantum systems. Computer Physics Communications, 183(8):1760–1772, 2012.
- [24] J.R. Johansson, P.D. Nation, and Franco Nori. Qutip 2: A python framework for the dynamics of open quantum systems. Computer Physics Communications, 184(4):1234–1240, 2013.
- [25] Alexander Lohrmann, Chithrabhanu Perumangatt, Aitor Villar, and Alexander Ling. Broadband pumped polarization entangled photon-pair source in a linear beam displacement interferometer. Applied Physics Letters, 116(2):021101, 2020.
- [26] Lana Sheridan, Thanh Phuc Le, and Valerio Scarani. Finite-key security against coherent attacks in quantum key distribution. New Journal of Physics, 12(12):123019, 2010.
- [27] Ian George, Jie Lin, and Norbert Lütkenhaus. Numerical calculations of the finite key rate for general quantum key distribution protocols. Physical Review Research, 3(1):013274, 2021.
- [28] Shihan Sajeed and Thomas Jennewein. Observing quantum coherence from photons scattered in free-space. arXiv:2103.00298 [quant-ph], February 2021. arXiv: 2103.00298.
- [29] Ali Anwar, Chithrabhanu Perumangatt, Fabian Steinlechner, Thomas Jennewein, and Alexander Ling. Entangled photon-pair sources based on three-wave mixing in bulk crystals. Review of Scientific Instruments, 92(4):041101, 2021.